SIMULATION OF CLIMATE ACROSS THE PERMIAN-TRIASSIC BOUNDARY WITH A FOCUS ON PHYTOGEOGRAPHICAL DATA ANALYSIS

by

MITALI DINESH GAUTAM

Presented to the Faculty of the Graduate School of

The University of Texas at Arlington in Partial Fulfillment

of the Requirements

for the Degree of

MASTER OF SCIENCE IN ENVIRONMENTAL SCIENCES

THE UNIVERSITY OF TEXAS AT ARLINGTON

December 2018

Acknowledgements

I would like to thank my advisor Dr. Arne Winguth for the opportunity and encouragement. I am thankful to the wonderful co-workers of the climate work group for their constant support, especially to Dr. Cornelia Winguth for her helpful insights for my thesis.

I am much obliged to my committee members for the precious time and inputs to my dissertation. I am indebted to my family and friends for believing in me and supporting my aspirations. I would like to thank Dr. John Connolly, data scientist from the office of information and technology, UTA for the help with statistical analyses.

Last but not the least, I would like to thank The University of Texas at Arlington for the financial support. I am grateful for the funding from NSF grant EAR 1636629. All the simulations have been carried out using the supercomputing facilities of the National Center for Atmospheric Research.

November 26, 2018

Abstract

SIMULATION OF CLIMATE ACROSS THE PERMIAN-TRIASSIC BOUNDARY WITH A FOUCS ON PHYTO-GEOGRAPHICAL DATA ANALYSIS

Mitali Gautam, MS

The University of Texas at Arlington, 2018

Supervising Professor: Arne Winguth

The present study aims at reconstructing the paleoclimate across the Permian-Triassic Boundary (PTB, 251.9 ± 0.024 Ma) which encompasses one of the major mass extinction events of the Earth's history. Results are analyzed from sensitivity experiments that have been previously been carried out with a community climate system model (CCSM3) for 4x CO_2 higher than the pre-industrial levels of 280 ppmv, 12.7x CO_2 and 12.7x CO_2 with a lower cloud cover . This study attempts to reconstruct the climate using the floristic patterns derived from plant-fossil data. Finally, simulated biomes are compared with data-derived biomes, in order to validate the amount of radiative forcing needed to reconstruct the climate across the PTB.

The climate simulations yield a rise in seasonality in surface temperatures over Pangea with increasing greenhouse gas concentrations. The simulations for precipitation predict large arid continental interiors and mega-monsoonal trends in the tropics. The change in floristic patterns follows the transitions into the extreme climatic conditions. The phytogeographical patterns show a coherence with the simulated climate. The

correspondence analysis indicates an association between the genera and localities co-occuring with each other. The discrepancies in the floristic patterns are being discussed. Reconstructed biome are in reasonable agreement with the biome inferred from time-slice climate simulations across the PTB. Consideration of higher model resolution and interactive paleovegetation dynamics in the climate model could lead to a reduction of model-data biases.

Table of Contents

List of Illustrations

List of Tables

Chapter 1

Introduction and Significance

Studies involving rapid climate transitions of the past are important for providing useful insights about the climate change. The present study examines the response of ecosystems to inhospitable conditions leading to a shift in biodiversity during a transition from an icehouse to the hothouse world. A prominent example of such a climate transition occurred from the late Paleozoic era to the early Mesozoic era (Rees et al., 2002). Within a narrow geologic time period near the Permian-Triassic boundary (PTB, 251.9 ± 0.024 Ma, Shen et al., 2011), there occurred a substantial perturbation of the Earth's climate that caused one of the most severe bio-crisis events of the Phanerozoic, leading to an extinction of more than 90% of marine species and approximately 70% of terrestrial species. (Erwin, 1994; Erwin, 2006; Retallack, 1995). The end-Permian extinction is of great interest because it is the largest and one of the first to be identified in the 26-million-year mass extinction cycle that aids in understanding the evolutionary role of mass extinction (Erwin, 1990). The present study addresses the seasonality changes across the PTB as inferred from climate-model simulations and their comparison to reconstructed phytogeographical patterns using a statistical analysis of plant-fossil data.

1.1 Proposed Causes of climate change across the PTB

The PTB was characterized by lethally hot surface temperatures and widespread ocean acidification, which is likely to have been caused by massive greenhouse gas emissions. Several causes for the catastrophic biotic event have been debated and proposed, including:

(i) The eruption of the Siberian traps, one of the largest continental flood-basalt provinces of the Earth (Renne and Basu, 1991; Campbell et al., 1992; Isozaki, 1997; Svensen et al., 2009; Payne and Clapham, 2012), and the related emission of greenhouse gases as well as methane hydrate release, leading to global climate change (Erwin, 1993; Wignall, 2001; Kidder and Worsley, 2004; Royer, 2006; Reichow et al., 2009; Svensen et al., 2009; Breecker et al., 2010).

(ii) The assembly of the super-continent Pangea which gave rise to high climatic continentality (Kutzbach and Gallimore, 1989).

(iii) An associated widespread ocean acidification due to ocean stratification (Wignall and Hallam, 1992; Kajiwara, 1994; Wignall and Twitchett, 1996; Isozaki, 1997; Kato et al., 2002; Kidder and Worsley, 2004; Payne and Clapham, 2012).

(iv) A bolide impact (Basu et al., 2003; Becker et al., 2004) that may have influenced the eruption of the Siberian traps (Kaiho et al., 2001), increasing the influx of carbon and light sulfur into the atmosphere.

1.2 PTB extinction / consequences

The catastrophic collapse of marine and terrestrial species is believed to have been linked to the consequences of one or a combination of the aforementioned causes.

Of all the proposed causes, the eruption of the Siberian traps has been considered as the primary trigger for the mass-extinction event. The massive release of carbon oxides and sulfur oxides (CO_2 and SO_2) from the Siberian traps could have exerted a considerable amount of global stress causing perturbations in atmospheric and oceanic chemistry. Based on numerous marginal gas explosion structures, Svensen et al. (2004) estimated that the degassing of the traps could have released about 100,000 GT (or 10^5 g) of carbon into the atmosphere. With CO_2 being a greenhouse gas, these emissions could potentially have led to a transition into a hothouse climate. In addition, the methane released from the basaltic magma would have consumed large amounts of atmospheric oxygen by oxidation to CO_2, thereby leading to a hotter climate and lower atmospheric oxygen levels. At the same time, the retreat of forests to the higher latitudes due to hot and arid environments would also have reduced the production of atmospheric oxygen as well as the uptake of CO_2, further exacerbating the existing greenhouse conditions. Furthermore, it is possible that the low-temperature surface fires and litter fires emanating from the existing dry conditions aggravated the destruction of terrestrial biota. Moreover, climate consequences of high CO_2 may have led to increased atmospheric water vapor content, a poleward moisture transport, and abundant rainfall at high latitudes (Manabe et al., 1994). The release of acid volatiles from the Siberian trap emissions into the atmosphere could also have been responsible for acid rain over the land as well as a lowered pH of oceanic waters. As a result of an accelerated hydrological cycle and acid rain, the prevalence of ocean anoxia might have been caused by increased chemical weathering rates on land. Additionally, findings by Svensen et al. (2009) and Visscher et al. (2004) suggest the release of organo-halogen compounds from the Siberian traps and an increased exposure to UV radiation which probably contributed to the collapse of terrestrial and marine ecosystems. The deteriorating

atmospheric conditions due to an exposure to UV radiation have also been related to the records of abnormal gymnosperm pollen morphotypes from localities in Russia and NW China as documented by Foster and Afonin (2005).

The increased seasonality due to larger continental masses could have led to the development of 'megamonsoonal' patterns around the PTB (Kutzbach and Gallimiore, 1989; Parrish, 1993). This could have affected nutrient availability contributing to ocean anoxia (Winguth and Winguth, 2013). However, a geologically rapid crisis of biodiversity is suggestive of eliminating a slow-process like the assembly of Pangea as a primary cause for the extinction event (Payne and Clapham, 2012).

All these consequences and feedbacks could have contributed to the cataclysmic extinction event across the PTB, which had the longest recovery period among Earth's extinction events (Retallack et al., 1995).

Chapter 2

Objectives

This study focuses on investigating the environmental changes and the related phytogeographic patterns in response to the perturbation in the radiative forcing across the PTB. A sophisticated, fully coupled climate-model simulation in conjunction with paleo-botanical, sedimentological as well as paleo-geographic analyses has been applied to understand the climate transitions and climate feedbacks that could have led to mega droughts and flooding contributing to the great dying event.

Although it is highly controversial what caused the largest biotic crisis event in earth's history, the evidence of massive greenhouse gas emissions associated with flood basalt volcanism could serve as a suitable analogue for understanding the implications of anthropogenic-induced future climate change.

The primary objective of this paper is to address the following questions:

i. How did the seasonality change across the PTB?
ii. How did phytogeographic patterns change due to changes in seasonality caused by aerosol and CO_2 radiative forcing?
iii. How much radiative forcing is required to simulate a climate consistent with the reconstructed biogeographic patterns?

Additionally, by reconstructing the past climate and correlating the resulting response of biota, the impact of the transition into a hothouse climate on the functioning of the bio-geochemical cycles (e.g. how the processes on land and ocean modulate the rate of CO_2 growth in the atmosphere) can be inferred which can also be compared to the present-day and future conditions.

Chapter 3
Methodology

3.1. Community Climate System Model Description and Boundary Conditions

A fully coupled comprehensive model, Community Climate System Model, version 3 (CCSM3; Collins et al., 2006), developed by NCAR has been applied for the PTB climate sensitivity experiments.

The model consists of four components: the atmosphere, land, ocean and sea ice, which are linked together through a central coupler (CPL6). The coupler exchanges the fluxes and states the information among these components (Collins et al., 2006; Yeager et al., 2006; Kiehl and Shields 2005). The atmospheric component, Community Atmospheric Model (CAM3), comprises of a spectral horizontal resolution of T31, corresponding to an equivalent grid spacing of about 3.75º x 3.75º in latitude and longitude with 26 vertical levels (Collins et al., 2006). It includes prognostic treatments of liquid and ice condensate; advection, detrainment, and sedimentation of cloud condensate; and separate treatments of frozen and liquid precipitation and a radiation code that contains new parameterizations for the longwave and shortwave interactions with water vapor (Collins et al. 2002, 2006). The prognostic sulfur cycle developed by Barth et al. (2000) and Rasch et al. (2000) for predicting sulfate aerosols derived from a three-dimensional assimilation (Collins 2001; Rasch et al. 2001) is used to calculate the direct effects of tropospheric aerosols on the radiative fluxes and heating rates (Collins et al. 2002). The land component, Community Land Model (CLM3) is integrated on the same horizontal grid as the atmosphere, with each grid box further divided into a hierarchy of land units, soil columns, and plant types. There are 10 subsurface soil layers in CLM3. The land units represent the largest spatial patterns of sub-grid heterogeneity and include glaciers, lakes, wetlands, urban areas, and vegetated regions (Collins et al., 2006). Based upon a nested sub-grid hierarchy of scales representing

land units, soil or snow columns, and plant functional types (Bonan et al. 2001; Olesonet al.2004), it also incorporates the modifications to increase the sensible and latent heat fluxes over sparsely vegetated surfaces. The new formulations incorporated in the model also derive the turbulent transfer coefficient form the canopy density instead of a constant value for high-density canopies, which is further used to derive the inputs for the calculation of latent and sensible heat fluxes (Collins et al., 2006). The ocean component, Parallel Ocean Program (POP), comprises of 3º horizontal grids with 25 vertical levels (Gent et al., 2006) and its first pole located at the South Pole and the second pole located over Greenland (Smith et al. 1995). The sea ice model, Community Sea Ice Model (CSIM), is integrated on the same horizontal grid as the ocean model (Collins et. al 2006).

The PTB boundary conditions considered in this study are listed in Table 3.1.1. and are discussed in the following (see Kiehl and Shields, 2005; Winguth et al., 2015).

Table 3.1.1. Boundary Conditions for Permian Simulations (adopted from Kiehl and Shields (2005).

	CO_2 (ppmv)	CH_4 (ppmv)	N_2O (ppmv)	S_0 (Wm^{-2})	Eccentricity	Obliquity
Value	3550	0.700	0.275	1338	0º	23.5º
Table adapted from Kiehl and Shields (2005); ppmv is parts per million by volume and S_0 is solar insolation						

The solar irradiance is adjusted to reflect a fainter sun in the past, with a value of 1338 Wm^{-2} which is 2.12% lesser than the modern value. The eccentricity is set to 0º, in order to represent an equal reception of solar radiation at both hemispheres, with an obliquity equal to the modern value of Earth's axial tilt (i.e. 23.5°). The paleogeography and paleotopography for the PTB are described in Kiehl and Shields (2005) and land surface types are adopted from Rees et al., (1999).

Two greenhouse gas levels are considered for the sensitivity experiments in this study. The 4x CO_2 levels higher than the pre-industrial concentrations (PAL, here forth) of 280 ppmv is considered to represent the estimates prior to the Siberian volcanism (assumed to resemble Wuchiapingian stage here). The 12.7x CO_2 PAL of 3550 ppmv is considered to simulate the end-Permian conditions (assumed to resemble Changhsingian stage here) based on the estimates from soil carbonate CO_2 paleo barometers by Kidder and Worsley, (2004).

The third sensitivity experiment incorporates a 12.7x CO_2 PAL with thinner cloud optical depth representing lower concentrations of aerosols with increased cloud droplet radius exacerbating the greenhouse condition (Winguth et al., 2015).The resultant scenario (12.7x CO_2_WC henceforth) representing the hothouse world is assumed to resemble the early Triassic concentrations. The concentrations of other greenhouse gases have been set to 0.700 ppmv and 0.275 ppmv for methane and nitrogen oxide respectively.

3.2. Data Compilation

The compilation and analysis of floral data for the present study is based on the approach as described by Rees et al., (2002). The compiled data is first used for the phytogeographical analysis following which a statistical analysis is applied to the data in order to test the relationship between the two nominal variables considered for the study.

The database comprising the taxonomic list has been gathered from the Paleo-Biology Database (www.paleodb.org, Rees et al., 2002) and from Osen (2014). The data selected for the analyses encompass the stages from late Permian (Changhsingian and Wuchiapingian) as well as early Triassic (Olenekian and Induan). The data are collected mainly from the stratigraphic papers (Rees et al., 2002) that also describe the criteria for inclusion and exclusion of the data in the database. According to these criteria, the fossil data based on leaf genera as well as stems and roots of only known affinities to the foliage as well as the members of the genera wherein the roots are more prominently preserved than any other foliage (like in lycopsids and sphenopsids) have been included.

On the contrary, in order to avoid replication, the reproductive organs of the members that depend on the leaf genera have been excluded from the analyses. Owing to the difficulties in recognition of foliage specific to each group from the analysis of impressions and compressions preserved within the fossils, the data has been categorized into the coarser morphological categories. As highlighted by Rees et al., (2002), working at species level entails uncertainties, hence, the floral lists were classified further only up to a genus level. It is very likely that the differences in the morphologies of the leaf specimen may arise due to growth at different position of the plant or other factors, causing the overestimation of species. The classification of such isolated specimen into different species may lead to errors and thereby, may hinder the standardized identification of floral data.

Conclusively, with the consideration that leaf morphologies depict the environmental adaptations, this data can assist in deriving broad vegetational patterns like the biome

distribution which remain largely undisturbed by the finer classifications into narrower groups. The final data comprises of 14 morphological categories with a total of 89 genera belonging to 6 main localities further divided into sub-regions (See Table 3.2.1.).

Table 3.2.1. List of localities and its sub-regions.

NUMBER	LOCALITY	CONTINENT/COUNTRY
1	Gondwana	(1) South America
		(2) Antarctica
		(3) Australia
		(4) Africa
		(5) India
		(6) Saudi Arabia
2	Angara	(7) Siberia
		(8) Russia
3	Mongolia	
4	China	(9) North China
		(10) South China
5	Euramerica	(11) Europe
		(12) North America
6	Other	

3.3 Phytogeographical Analysis

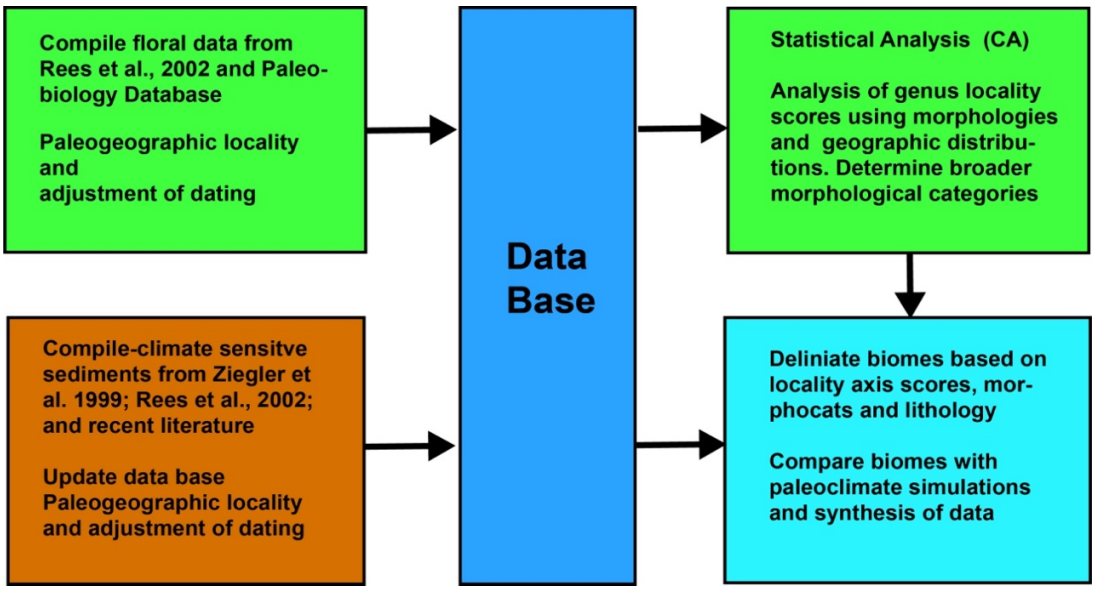

Figure 3.3.1. Methodology for the reconstruction of Biomes across the PTB (adapted from Rees et al., 2002).

The primary goal is to compile the global phytogeographic patterns across the Permian-Triassic boundary using the fossil floras (see Figure 3.3.1.).

Using paleo-botany, it is possible to state the patterns of changes in climate during the past i.e. changes during the cooling and warming periods, aridification and humidification, an increase or decrease in seasonality of climate (Meyen, 1987), etc. Since each floral category is specific to certain environmental conditions, such compilation can considerably contribute to the interpretation of the past terrestrial climate. For example, the westward spread out of Cathaysian realm (tropical flora) during the late Permian, with its localities in Turkey, Iraq, Saudi Arabia and Syria, suggests the existence of temperature- and moisture- dependent flora (thermophilic and hydrophilic respectively) along the Tethys coast (Meyen, 1987).

The combined information from the paleo-botanical database as well as the lithological indicators like the climate-sensitive sediments can enable a robust and refined interpretation of the climate changes across the PTB for the future studies.

For the paleo-phytogeographical analysis, the study follows a system of present-day distinct biomes as defined by Ziegler (1990) that can be applied to past.

Biomes are defined as the world's major communities, classified according to the predominant vegetation and characterized by adaptations of organisms to that particular environment**.** The distribution of terrestrial biomes is highly dependent on temperature and precipitation, as can be inferred from Figure 3.3.2. The temperature is relatively uniform in the low latitudes like tropical and low-temperate regions, and hence, the biome distribution is more dependent on the precipitation. On the contrary, the high latitude biomes are mainly dependent on temperature and the related growing seasons (Ziegler 1990, Rees et al., 2002).

The ten biomes described in Table 3.3.1., are defined by Ziegler and adapted from the criteria used by Walter (1985) that originally comprises of 9 biomes. The scheme presented by Walter to divide the macro-climate, was developed using 8000 meteorological ground stations worldwide. However, it is to be noted that the nature of boundaries between the biomes are gradual, rather than being sharp and distinct, and the same is applicable for the past biomes. Also, the assignment of Permian floras to the present-day biomes, must assume that the response of plants to the climate stringencies is coherent with the one observed today.

Three floral realms of Permian have been described by Ziegler (1990), for the paleo-flora. These are the south temperate Gondwanan Realm of central Gondwana, the tropical Cathaysian Realm of equatorial Gondwana, Laurasia and south Asian micro-continents as well as the north temperate Angaran Realm of Siberia and Kazakhstania, that were differentiated due to an increasing equator-to-pole gradient as well as the two great subtropical deserts acting as barriers to floral interchange.

The present study uses the information about the properties of biomes (see Table 3.3.1.) described by Ziegler, (1990) as has been extracted for the paleogeographic purposed from Walter, (1985).

The paleo-floristic patterns for the current research have been delivered using the pie-charts that comprise the morphological categories from the database, overlain at the respective paleo-coordinates.

The sizes of the pie-charts represent the diversity of genera within the morphological categories. Thus, the bigger the size, higher is the diversity within the respective locality. This is particularly important as, with the transition into the hothouse world in early Triassic, the terrestrial biota may have been exposed to increased environmental stress, leading to its extinction. Hence, the hotter climates are expected to have eliminated or lowered the diversity. In addition, a shift in the flora that is capable of thriving in relatively arid conditions and is tolerant to seasonal stresses from the ones that are less tolerant requiring an optimal to lower temperature as well as precipitation is expected.

Table 3.3.1. Climates and biomes inferred from temperature (T) and precipitation (P) adapted from Walters Scheme and its Permian equivalents, modified from Ziegler (1990) and Rees et al., (2002).

Number	Climates	Modern vegetation	Permian biomes	# of Months	
				T>10 °C	P≥20mm
1	Tropical, humid	Tropical rain forest	Tropical ever wet	12	11-12
2	Tropical, humid summers	Tropical deciduous forests	Tropical summer wet	12	4-10
3	Subtropical, arid	Desert	Desert	11-12	0-3
4	Warm temperate, dry summers	Sclerophyllous woody plants	Winter wet	11	5-10
5	Warm temperate, humid	Temperate evergreen forests	Warm temperate	11	11-12

Table 3.3.1.continued

6	Cool temperate	Nemoral broadleaf deciduous forest	Cool temperate	5-6	5-10
7	Cool temperate, dry summers	Steppe	Mid-latitude desert	3-10	0-5
8	Cold temperate	Boreal conifer forest	Cold temperate	2-4	2-12
9	Arctic	Tundra vgetation	Tundra	0-1	---
10	Polar/Glacial	Ice-sheets	Polar	0	---

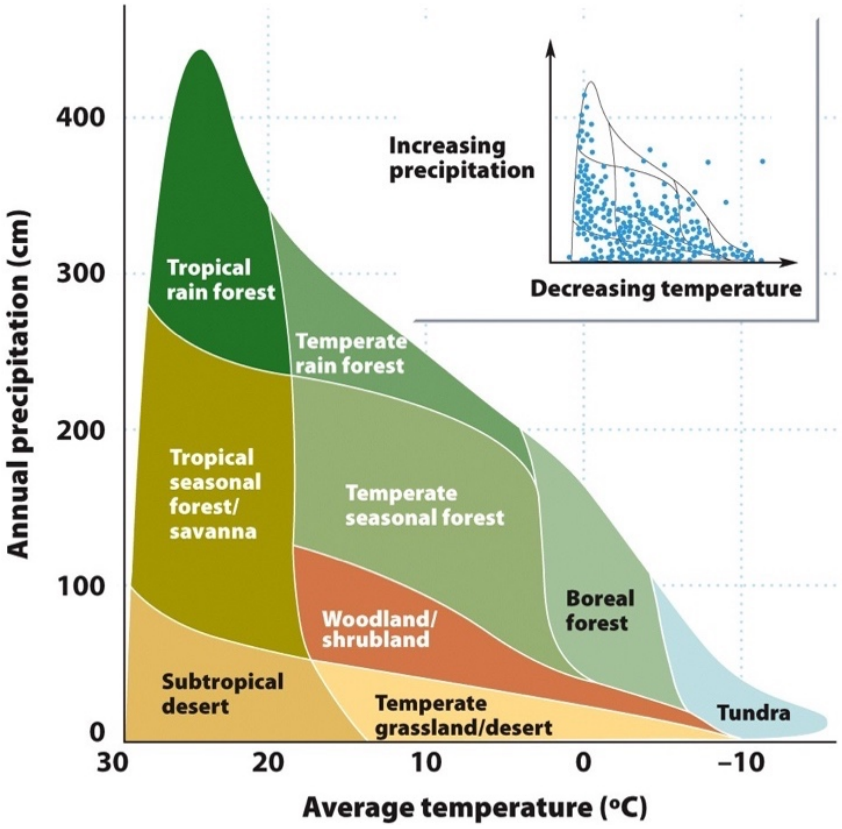

Figure 3.3.2. Differentiation of Biomes based on the mean annual temperature and precipitation (R.H. Whittaker, Communities and Ecosystems, 2nd ed.,Macmillan, New York ,1975).

3.4. Correspondence Analysis

The ecological aspects of a community consist of the organisms inhabiting an ecological space and its relationships as well as interactions with the respective environmental factors. The community data (plant fossil data) for the present study is multivariate like most community datasets, as, each sample is described by the abundance of the genera based on the environmental conditions, affecting its distribution. A multivariate analysis technique is applied to the data in order to examine more than one variable simultaneously. The purpose of the multivariate analysis is to treat the multivariate data as a whole in order to summarize and interpret its structure based on the environmental factors. This application of statistics aims at improvising the comprehension of the data and interpret the patterns of floral distribution in an effective way.

As specified in the previous section, the present study utilizes the plant fossil data as a means to interpret the past climate. With the application of statistics, the study aims to corroborate the ability of the use of floral data to investigate the large-scale climate information. A statistical analyses is recommended to avoid biased correlations between the relevant varaibles (Hu et al.,2017) and to assess uncertainties.

In this study, genera across the PTB boundary correlated with various localities to interpret and pytogeographic patterns and associated biome across the PTB. In general, the distribution of plants is based on multiple factors. However, Ziegler (1990) has discussed a close association of the plants found at respective localities based on the climatic conditions. He further categorized the various localities into distinct floral realms, as described in the previous section, that comprises of the specific plant types.

In order to test the statistical significance of the data, the present study proposes a null hypothesis (H_0) which assumes that the variables under study are not correlated and that no association between the co-occurrence, if any, exists. The alternative hypothesis (H_a) thus implies that there is a significant correlation between the variables of the dataset i.e.

they co-occur as the distribution of plants is largely dependent on the prevalent climatic conditions, and thus locality. Hence, the floral data is statistically tested for a correlation between the two variables (genera and localities) with a significance level of 5% (p-value of 0.05).

Correspondence analysis (CA), an ordination technique following the work of Rees et al., (2002) is applied for the statistical analysis. It is convenient to summarize the high-dimensional field data (due to the large numbers of samples and species) into a low-dimensional ordination space (usually one to three dimensions) using CA wherein the similar genera and localities plot close together and vice versa. For example, the localities of Cathaysian floral realms (tropical/ever wet to mid-latitude deserts) sharing similar climatic conditions like north-south China and Arabia are expected to plot closer to each other. Similarly, members of same morphological categories, will be plotted closer to each other owing to their similarities. A relationship between the distinct genera and localities can be inferred too. For example, the fern-like vegetation should be expected to plot closer to tropical localities.

Data Analysis: The correspondence analysis, also known as Reciprocal Averaging (Hill, 1974) has been carried out using SPSS software. It is termed so, because the species ordination scores are averages of sample ordination scores and vice versa (i.e. there exists a 'reciprocal' relation between the two).

The algorithm of CA involves a simple matrix formula (Gauch, 1982). As suggested by its name, using the iterations, at first, the algorithm assigns arbitrary species (or sample) ordination scores based on which, the sample (or species) scores are derived. In the second iteration, the new species scores are derived based on the sample scores obtained from the first iteration. Subsequently, the following iterations progresses until the solution convergences. The eigen values is a measure how will the genera corresponds to the localities while transforming the data into a lower dimensional space. Thus, the magnitude

of eigenvalues of an axis is directly proportional to corresponding correlation of genera and locality.

The variance shown on the first axis is higher than the subsequent axes, which account for lesser variance gradually. This technique also allows the organization of the data for interpreting the floristic patterns for the plots of variables under examination on a same scale (Gauch, 1982) and in turn, directly compare them if found to be statistically significant. Here, we limit the analysis to the most dominat correlations on the first four axes, in particular the first two axes.

Chapter 4

Results

4.1 Results from Permian Climate Simulations

In the following section, seasonality of the CCSM3 simulations are discussed. Figure 4.1.1 shows simulations for the surface air temperature developed for 4x CO_2 scenario for the four meteorological seasons: boreal winter (DJF), spring (MAM), summer(JJA), and fall (SON). Over Angara, surface temperature ranges from ranges to ~40 ºC from -10 ºC for the winter and as high as bout 30 ºC for summer. Even more extereme temperature ranges are simulated over the interior of Gondwana (Figure 4.1.2.). The seasonal range exceeds 50 ºC with -30 ºC in the winter to 20 ºC in the summer.

The seasonal cycle is amplified by a few degrees over Angara and Gondwana in the 12.7x CO_2 experiment compared to the 4x CO_2 scenario. In the 12x CO_2 scenario, extreme high temperatures reach 45 ºC over Laurasia and northern Gondawana due to the increase in greenhouse gas forcing and reduced latent heat release.

The 12.7x PAL CO_2_WC scenario represents a transition into the hothouse world (Figure 4.1.3). For most continental interiors, the higher temperatures of about 40ºC-45ºC are simulated and the higher latitudes are ice-free.

Hence, an increase in summer temperatures as well as a weakening of winter temperatures can be observed. Gondwana summer surface temperatures are 55ºC in the subtropics and ~-20ºC during the Gondwana summer. The temperature range over Angara is more moderate.

The equatorial regions for all sensitivity experiments show an increase of about 5ºC subsequently as we move from 4x PAL CO_2 to 12.7x PAL CO_2_WC.

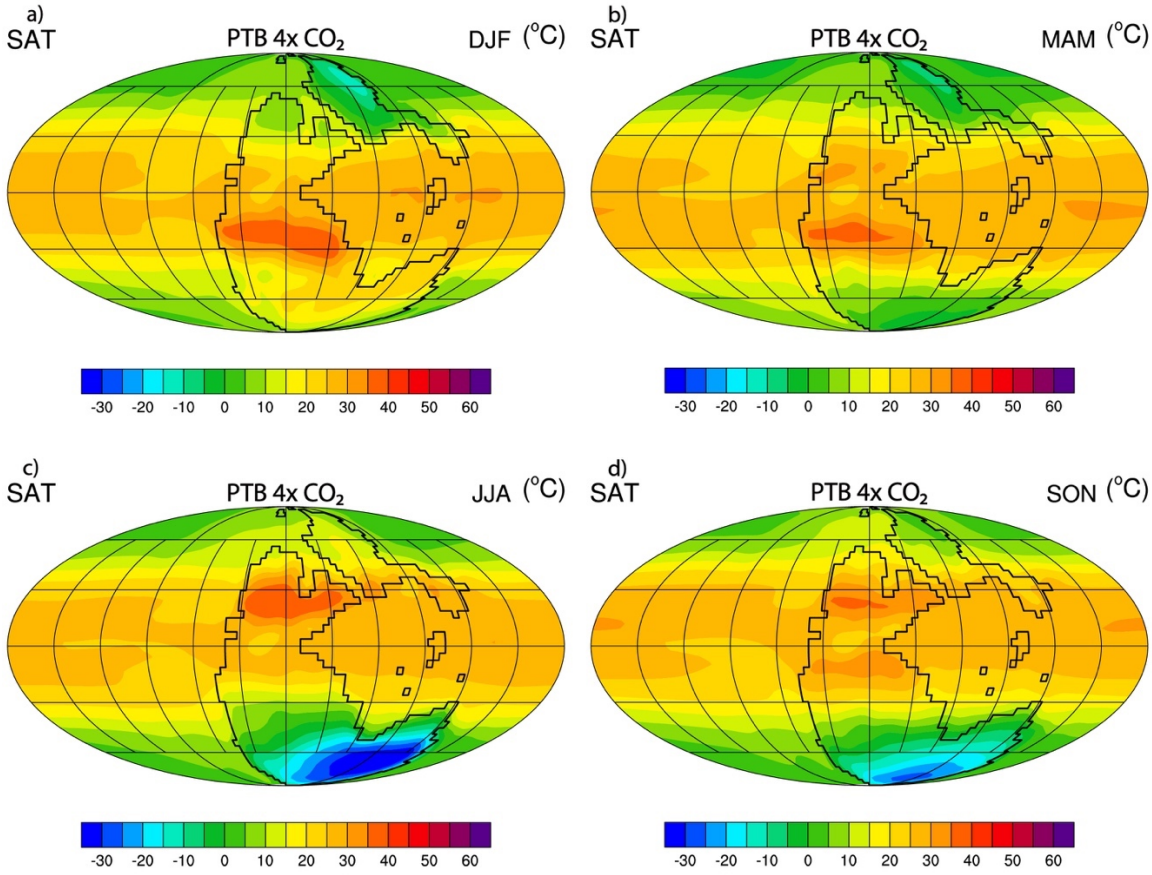

Figure 4.1.1. Seasonal PTB surface air temperatures derived from a 4x PAL CO_2 CCSM3 simulation for boreal a) winter, b) spring, c) summer, and d) fall.

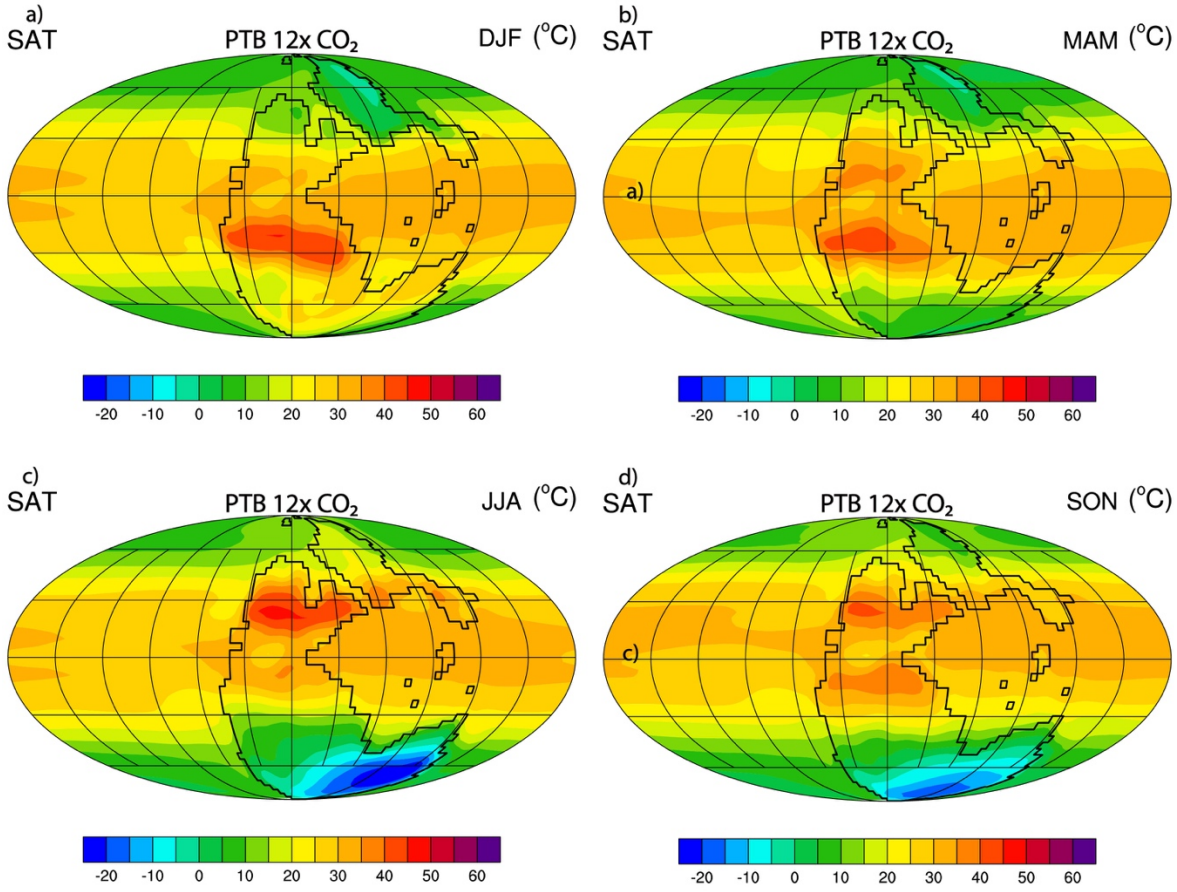

Figure 4.1.2. Seasonal PTB surface air temperatures derived from a 12.7x PAL CO_2 CCSM3 simulation for boreal a) winter, b) spring, c) summer, and d) fall

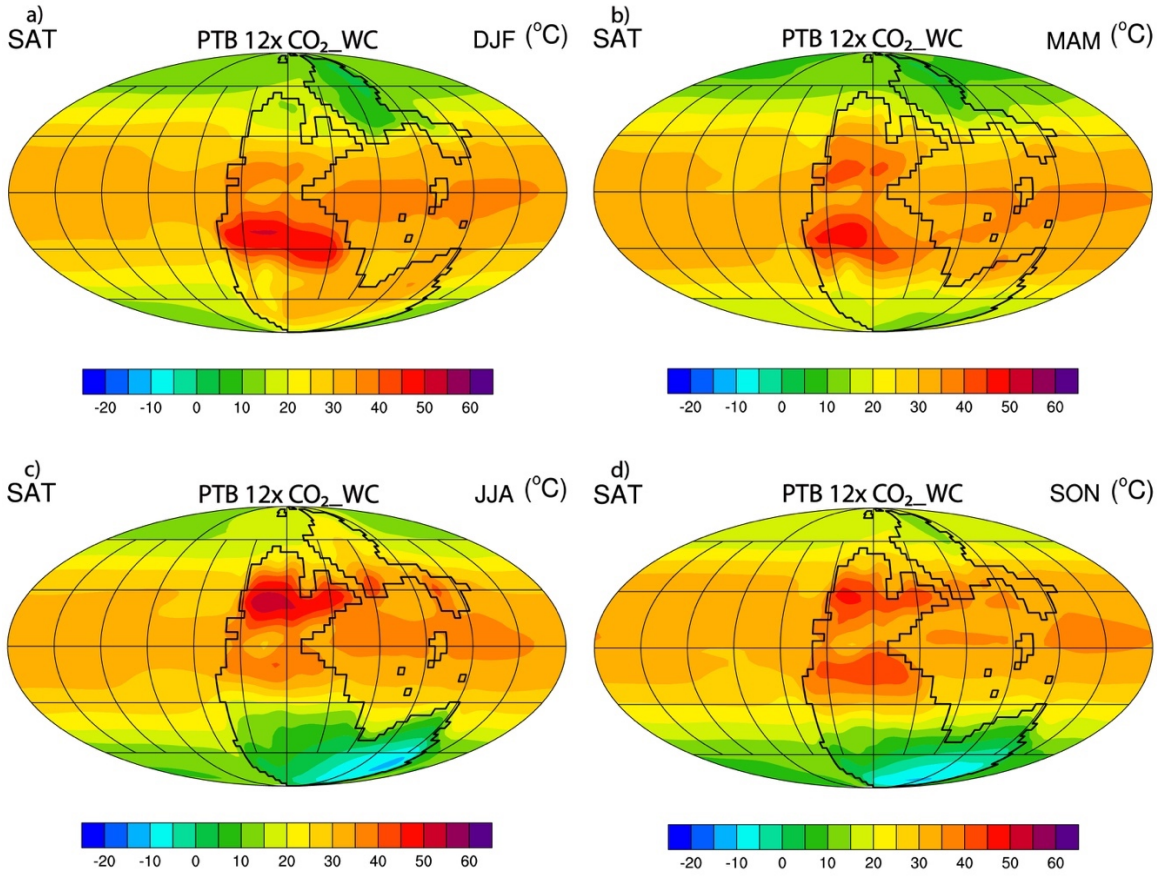

Figure 4.1.3. Seasonal PTB surface air temperatures derived from a 12.7x PAL CO_2_WC (with lower cloud optical depth) CCSM3 simulation for boreal a) winter, b) spring, c) summer, and d) fall .

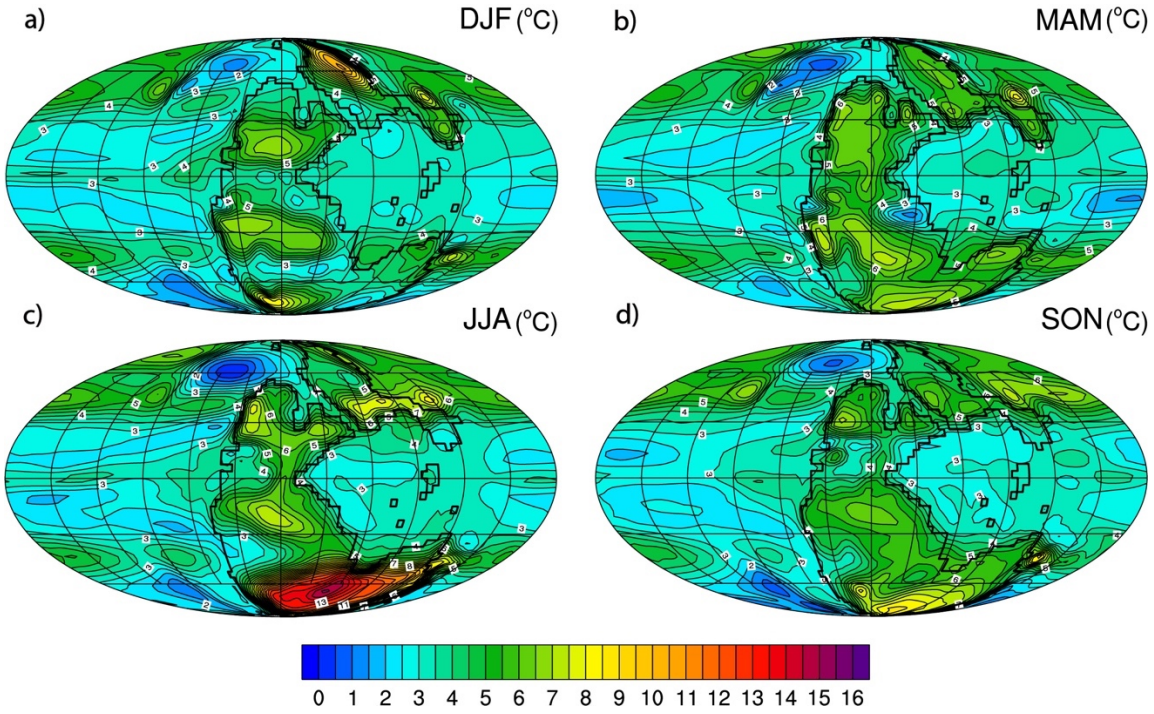

Figure 4.1.4. Difference in PTB surface air temperature between the 12.7xCO_2 PAL and 4xCO_2 PAL simulated by CCSM3 for boreal a) winter, b) spring, c) summer, and d) fall.

Figures 4.1.4. and 4.1.5. display the difference in seasonality of surface temperatures between the 12.7x CO_2 and 12.7x CO_2_WC experiments compared with 4xCO_2 levels. The winter temperature in the northern hemisphere increase in temperatures by 10 ºC, whereas the summers are intensified by about 8ºC for 12.7x CO_2 as compared to 4x CO_2 scenario. This difference is even rises to 16ºC and 10ºC respectively, if the 12.7x CO_2_WC is compared with the 4x CO_2 scenario (Figure 4.1.5). The summers of southern hemisphere, increase by 9ºC and the winters get warmer by about 15ºC for 12.7x CO_2 as compared to 4x CO_2. A substantial higher temperatures of 2ºC in summer and 27ºC in winter is predicted by the difference between the 12.7x CO_2_WC with the to 4x CO_2 experiment.

Figures 4.1.6 show the seasonal differences for precipitation-evaporation for the low greenhouse gas concentration (i.e. 4x CO_2) experiment. Evaporation exceeds precipitation over most of the continental interior in the summer hemisphere whereas, only a narrow belt in northern tropics and polar coast are the exceptions. In the winter hemisphere, such scenario (E>P) is observed equator-ward at about 25˚ latitude. This shows coherence with the observational studies of the past which are validated by the presence of evaporites in the respective regions (Kutzbach 1989). However, with even higher CO_2 levels and altered cloud optical depth, we not only see an intensification of the monsoonal circulations, but also an expansion of mega-monsoonal pattern across the tropics as well as higher latitudes (see Figure 4.1.7.).

Figure 4.1.8. represents seasonal temperature and precipitation trends in Australia for 4x CO_2, 12.7x CO_2,12.7x CO_2_WC. As can be inferred from the plots, the precipitation almost doubles (~35mm/month for 4x CO_2 to ~67mm/month for 12.7x CO_2 _WC) during the summer (DJF) with increased radiative forcing. The winter temperatures and precipitation show an increase too. This trend may be explanatory for the ice-free higher latitudes and the presence of temperate vegetation as will be discussed in the sections further.

Similarly, Figure 4.1.9. representing seasonal temperature and precipitation trends in South China, a tropical locality, depicts a relatively stable temperature over all months, as expected. However, interesting trends in precipitation can be observed with increasing CO_2 forcing. It is expected that owing to the mega-monsoonal trend that, the rainfall should be increasing in summer. Contrary to this, we see a decrease possibly due to a disruption of the low-pressure system by the surrounding high-pressure system over Panthalassa followed by an increase during early Triassic. This can be attributed to a localized effect rather than a global trend.

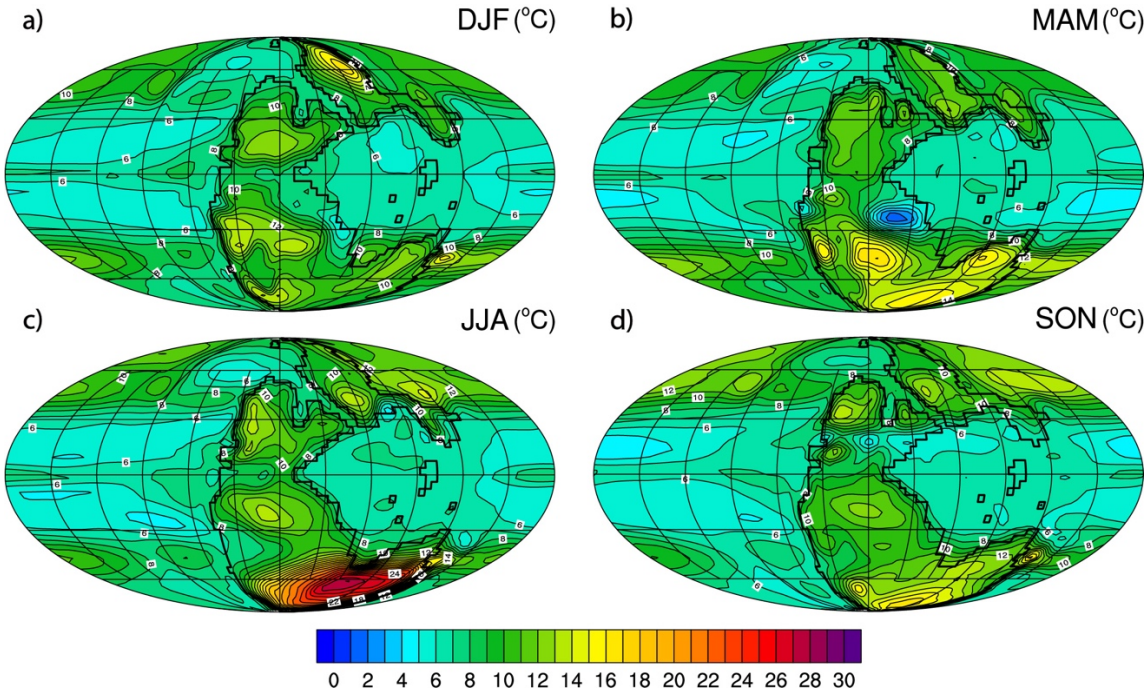

Figure 4.1.5. Difference in PTB surface air temperature between the 12.7xCO_2 PAL_WC and 4xCO_2 PAL simulated by CCSM3 for boreal a) winter, b) spring, c) summer, and d) fall.

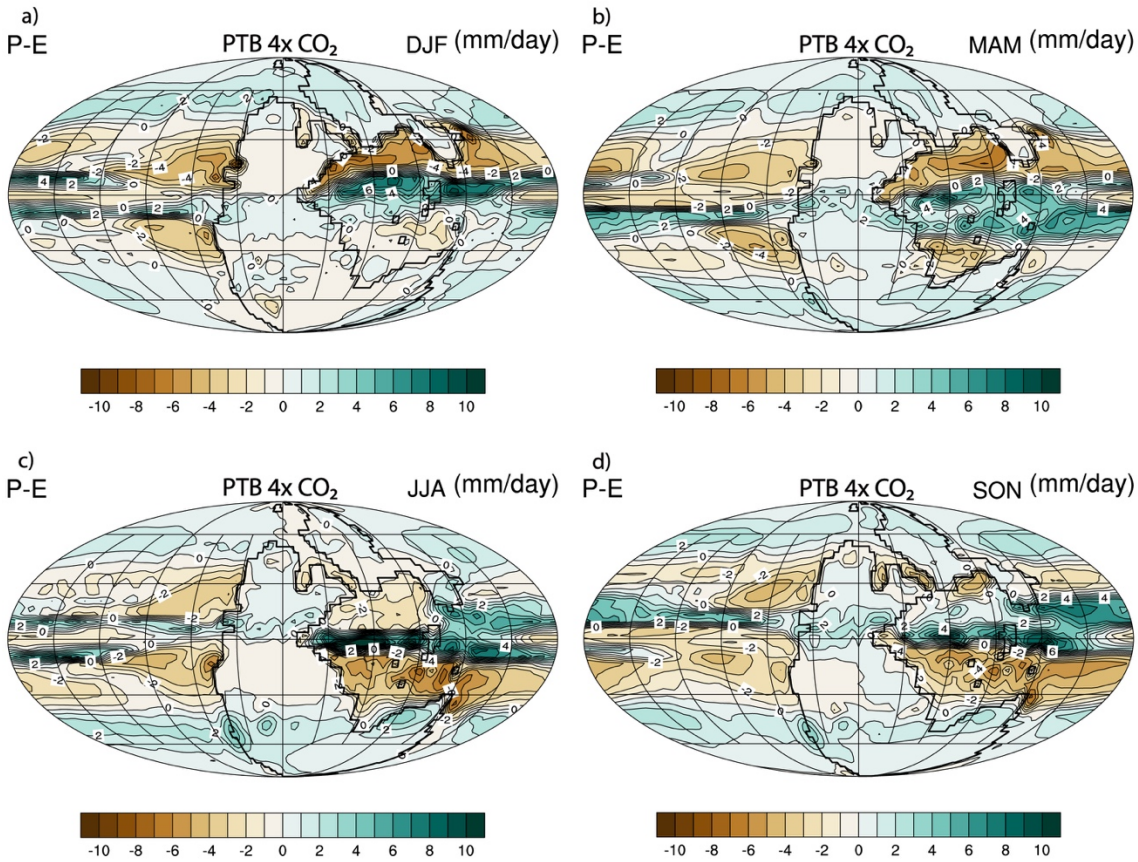

Figure 4.1.6. Seasonal PTB precipitation-evaporation (P-E) from a 4x PAL CO_2 CCSM3 simulation for boreal a) winter, b) spring, c) summer, and d) fall.

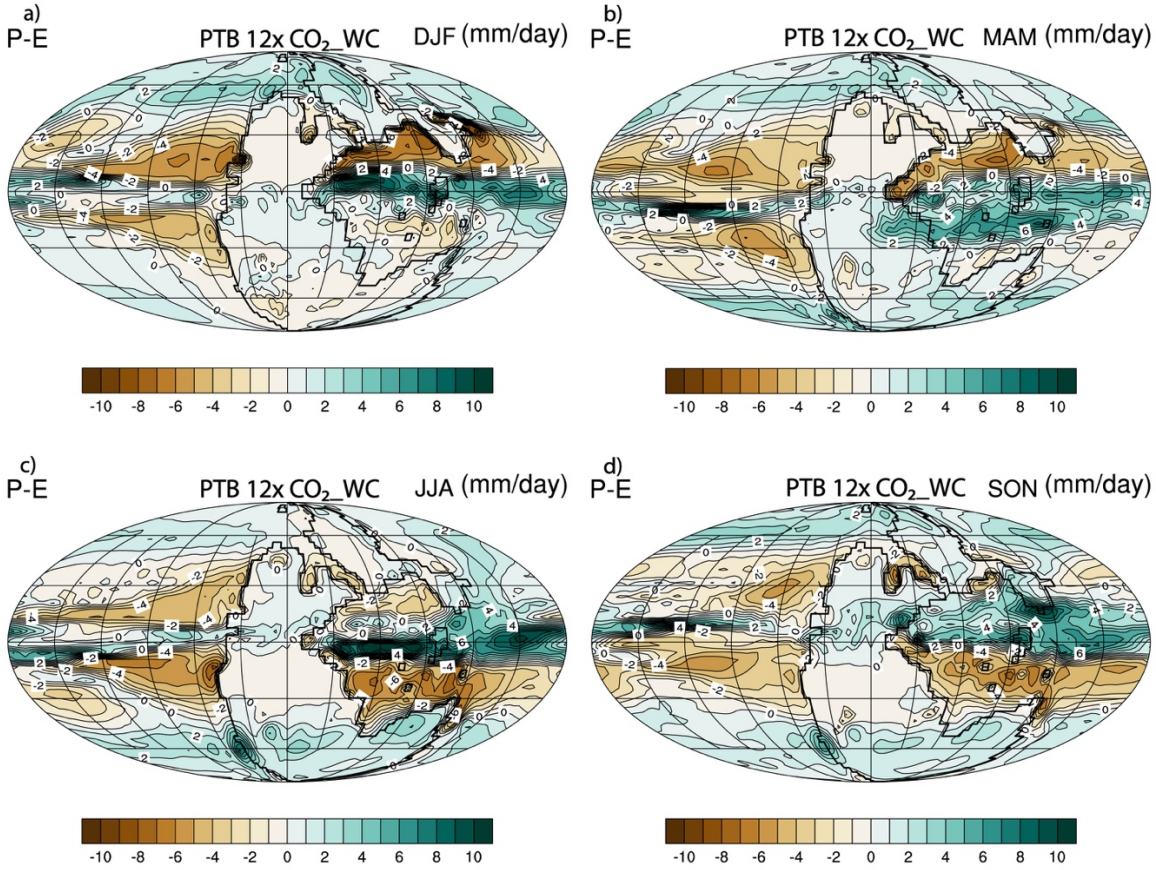

Figure 4.1.7. Seasonal Precipitation-Evaporation (P-E) from a 12.7x PAL CO_2 and lower cloud optical depth CCSM3 simulation for boreal a) winter, b) spring, c) summer, and d) fall.

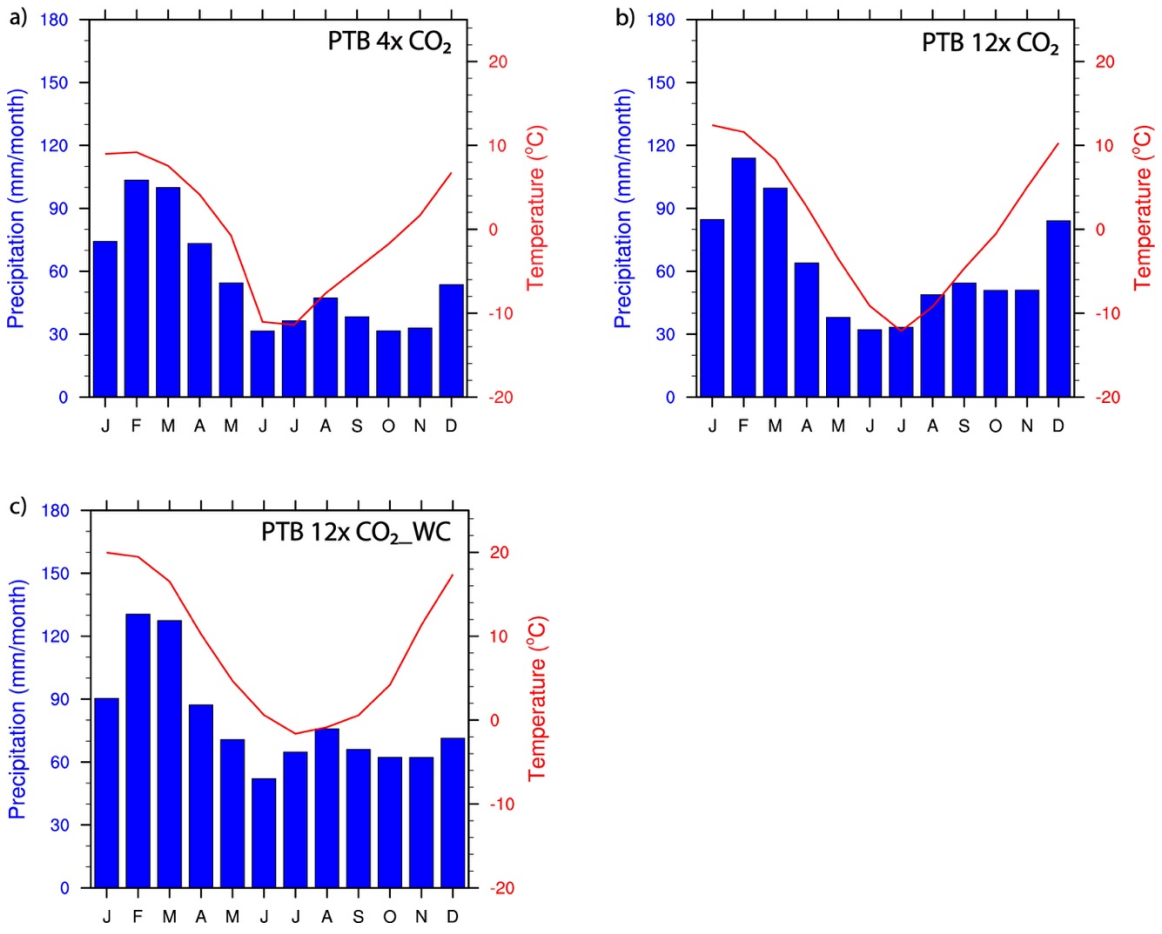

Figure 4.1.8. Seasonal temperature and precipitation trends in Australia for 4xCO_2, 12.7x CO_2, and 12.7x CO_2_WC scenarios.

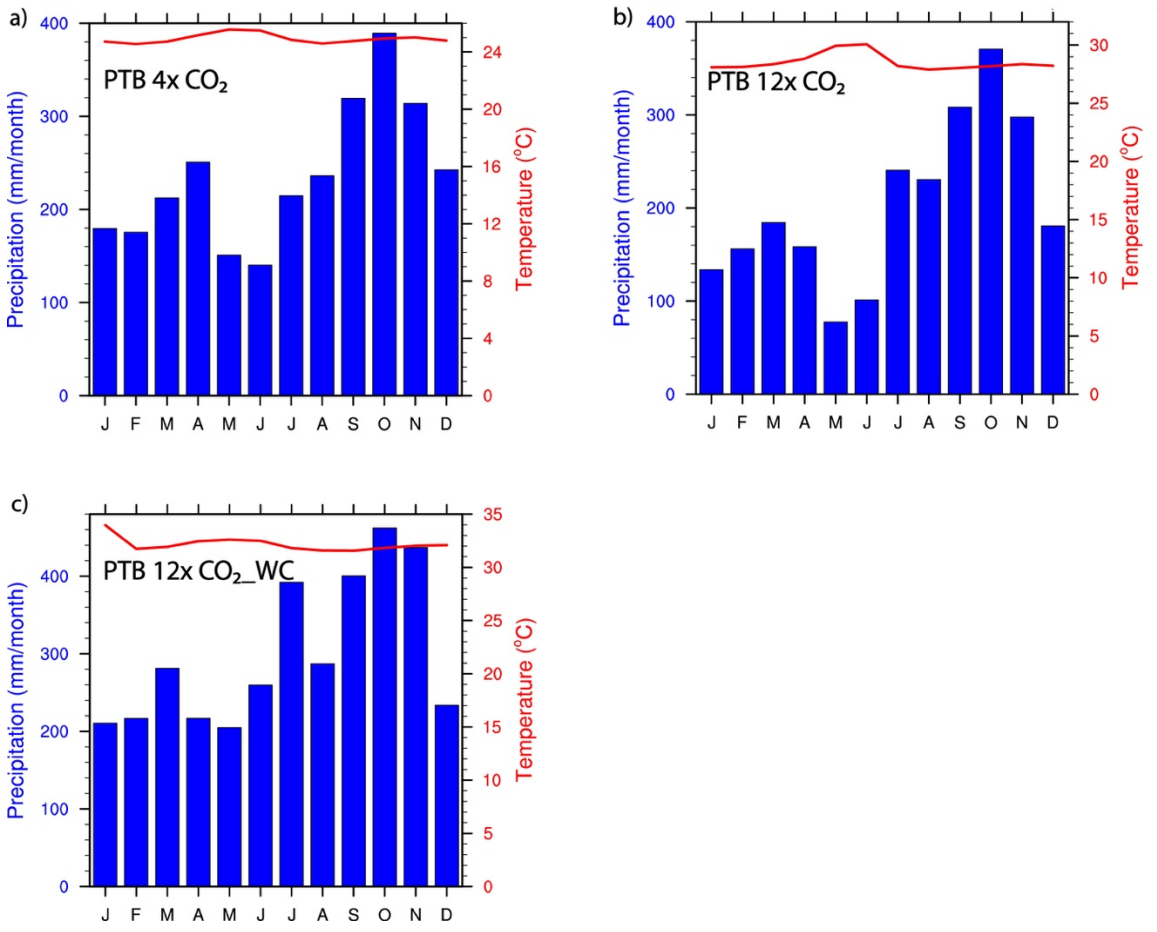

Figure 4.1.9. Seasonal temperature and precipitation trends in South China for 4x CO_2, 12.7x CO_2, and 12.7x CO_2_WC scenarios.

4.2 Phytogeographical patterns using the plant fossil data.

In the following section, the biomes simulated using the CCSM3 model are discussed which are compared to the derived floristic patterns using the fossil-data.

The 4xCO_2 levels [Figure 4.2.1. (a)] simulate a narrow band of tropical biomes near the equator along the ITCZ and eastern coast of north China, followed by arid belts of seasonally wet, deciduous summer-wet biomes along its margins. The summer-wet biomes comprise a part of Euramerica localities, north China as well as Arabia. However, embedded in between are the desert biomes (tropical deserts), characterized by drier areas of the descending Hadley cell occurring ~15°-35° north and south as well as some regions along the west coast and cold regions of upwelling that inhibit precipitation. The winter-wet biomes are not extensively developed except for some possible rain shadow regions in north and south. The warm-temperate biomes are simulated in the regions that comprise of temperatures above freezing during the winter months as well as sufficient rainfall, to harbor the related evergreen vegetation. Regions from northern Greenland through some regions near the Urals, south east coast of Soviet Union simulates these biomes for 4xCO_2 levels. The midlatitude deserts are simulated for some continental interiors in mid-latitudes that were too remote from the moisture sources or isolated by rain shadows (like the African regions). However, the higher latitudes simulate the cool and cold temperate biomes with lower CO_2 scenario for frosty winters as well as regions of low to moderate rainfall experiencing lower evaporation rates like the low-lands of Siberia in North as well as Autralia and Antarctica in South. The small regions of the Tundra biome are simulated near the north and south pole by the mountain ranges.

The floral distribution for the Wuchiapigian stage have been plotted over the biomes derived from 4xCO_2 levels. The size of the pie-charts represent the diversity of genera at repective localities. As seen in the figure, we donot see an occurrence of Conifers for any of the stages. The Cathaysian realm shows a higher diversity of flora, specifically, south

China and the associated micro-continents due to the tropical and diversity-favoring conditions, as expected. The Ferns along with Pteridosperms that tend to appear in tropical to warm temperate regions, are extensively found in the low to mid latitudes. North and south China show a record of these floral groups. Sphenopsids (probably in its herbaceous forms) is widely distributed in the Cathaysian realm in the south Chineese as well as Euramerican localities. Cycadophytes and Peltasperms show a dominant occurrence in these localities extending from low to mid latitudes favoring the rain forest (like in south China) to environmentally stressed situations (like in Europe). Ginkgophytes, expected to be closely associated with them are not recorded in the data, probably due to lack of identification with certainty. Not many occurences of Pinales are found in Wuchiapingian, except for the ones in Euramerica representing a transition into the arid belts. The Lycopsids are most abundantly found in the low-latitude tropics, by the equator (in Chineese microcontinents), as also has been supported by Rees et al. (2002). The Angaran realm, which, from the biome simulations represent the high latitude north temperate regions as well as the south temperate Gondwanan realm, show a relatively lower occurrence of flora. Like the Cathaysian realm, the Angaran realm shows a predominant occurrence of Cordaites, a characteristic flora of cold-temperate, higher latitudes. The high-latitude locality like Australia of the Gondwanan realm shows some records too. The Cordaites show a versatile distribution due to a wide variety of growth habitats ranging from bushes and mangroves to large trees (Stewart 1983). Most likely, the Shenopsids occurred in herbaceous forms at the higher latitudes, as, these flora generally belong to low-mid latitudes. The Ferns show a wide adaptability in terms of environment. They are not only found in the wetter tropical realms, but also in the seasonally stressed high-latitude realms like Siberia and Autralia. However, Glossopteris is found to be dominant in the south-temperate high latitude locality of Autralia.

The 12.7x CO_2, as suggestive of higher radiative forcing simulates a broader tropical belt [Figure 4.2.1. (b)], in agreement with increased surface temperatures and increase in

rainfall, in the tropics. Similar to the 4x CO_2 scenario, the margins of tropics are characterized by the summer-wet biomes, which show expanded arid belts indicated by the tropical desert belts due to increased aridity as a result of higher radiative forcing. The simulated temperate deserts in the mid-latitudes for the 4x CO_2 scenario are replaced by the summer-wet biomes in the 12.7x CO_2 as a result of intensified monsoonal circulations. A major difference in the simulated high-latitude biomes with 12.7x CO_2 can be observed compared to 4x CO_2 scenario. With the weakening of winter cooling, the temperature-dependent, high latitude biomes show a shift towards the warmer biomes. The warm temperate biomes ~30°-45° are simulated in the south as well some coastal regions of Australia. A replacement of temperate desert by an expanded belt of Winter-wet biomes in Africa can be observed too. Similarly, the cold temperate biomes simulated at the higher latitudes for 4x CO_2 levels, reduce substantially with a higher area for the relatively warmer, cool temperate biomes simulated for the 12.7x CO_2 scenario. The uplands of Siberia, Antarctica and Autralian regions are indicative of such change in biomes.The coverage of Tundra biomes simulated for 4x CO_2 is eliminated from northern as well as southern pole with higher levels of greenhouse gas forcing.

The floral distribution of the Changhsingian stage [Figure 4.2.1. (b)] representing the end-Permian conditions, shows a significant reduction in the number of occurences recorded. The Ginkgophytes show a predominant occurrence in the mid-latitude north Chineese locality belonging to the Cathaysian realm. Although, the floral groups are almost the same as the ones discussed for the Wuchiapingian stage, the diversity found in most localities shows a significant decline. Also, while progressing to warmer conditions, an increase in the precipitation in the tropics is expected to increase the diversity. However, a localized effect possibly disrupting the low-pressure cell over south China, responsible for causing a decrease in precipitation could be a plausible explanation for the reduced diversity observed over that region. The floral groups in the Cathaysian realm thus comprises of Ferns, Pteridosperms, Gigantopterids as well as some Sphenophytes,

Peltasperms and Cordaites.The floral groups belonging to Fern3 as well as Lycopsids seem to disappear. The recorded flora from the Siberian locality during Wuchiapingian seems to disappear or become extinct in the Changhsingian stage. The floral groups in Euramerica only comprise only of Peltasperm and Ferns, with a suggestive disppearence of Cordaites, Cycadophytes, Sphenopsids, and Pteridosperms. On the contrary, the north China shows a drastic increase in the diversity relative to other regions. This could be reflective of the northward shift of flora over time with the warming of higher latitudes. The Ferns, a dominant genera of the warm temperate regions, has been extensively recorded from the data. Other recorded floral groups include Cordaites, Sphenopsids Pteridosperms as well as Peltasperms, that prefer the aforementioned habitats. In addition to north China, Africa belonging to the Gondwanan realm shows a slight increase in the number of occurences as well as diversity. Sphenophytes, indicating the warming of climate is recorded along with some Glossopterids and Cordaites. The Cordaites and Glossopterids showing an affinity towards the cool temperate habitats dominate the localities of Autralia. Smaller and herbaceous forms of Sphenopsids are extended to the highest latitudes suggestive of a warming trend too.

Finally, as we simulate the biomes for 12.7x CO_2_WC scenario [Figure 4.2.1. (c)], a higher increase in the tropical biomes is simulated.This is observed in the western coast along the Afro-american region, some regions on the eastern coast of Tethys as well as lowlands of Siberia. According to the simulations, the sub-tropics and mid-latitudes (till about 45° north and south) are mainly characterized by the summer-wet biomes with some desert biomes in between. The winter-wet or temperate biomes, as simulated in the previous scenarios, for these regions, is almost eliminated. The higher latitudes from about 45° onwards, simulate warm temperate biomes, followed by the cool temperate biomes. This distribution coincides with the above-freezing temperatures and sufficient rainfall recorded for all seasons in case of the warm climate scenario of increased greenhouse gas levels. The wet-summers for regions like Australia, and northern parts of north China,

explain such biome distributions. The cold temperate biomes are completely eliminated for the present scenario, with the resulting warmer and wetter climate, as per the simulations.Thus, the warmer biomes simulate at the relatively warmer high latitudes as suggested by the geologic evidences and previous literature.

The floristic patterns of early Triassic stages suggest the transition into a hothouse climate as we see a substantial decline in diversity, possibly due to the inhospitable conditions. The Cathaysian realm shows a distribution of flora in the south as well as north China and Euramerica. South China is mostly dominated by Ferns with a fewer Sphenopsids and Cordaite. Similarly, north China shows a dominant occurrence of Ferns too. However, Gigantopterids, Cordaites, Spehnopsids and Cycadophytes that show a wide ranging preference in terms of habitat co-occur with the Ferns. The Euramerican locality seems to have shifted to relatively hotter and seasonally stressed conditions favoring a dominance of Ferns (majority), Sphenopsids and Cycadophytes which are known to have a high adaptability to seasonal-stresses. The southern Gondwanan realm shows a predominance Pinales in association with Glossopterids, Cycadophytes which diversified in warmer climate and some Ginkgophytes suggesting warm to cool temperate habitats. Although there have been evidences of disappearance of Glossopterids during early Triassic, some data has been found over India and Antarctica.

The disappeared flora over Angara in Changhsingian, reappears with a diversity of flora consisting of Ferns, Sphenopsids, Ginkgophytes and Cordaites. It is possible that with the warming of the poles an increased number of occurences as well as diversity is observed.

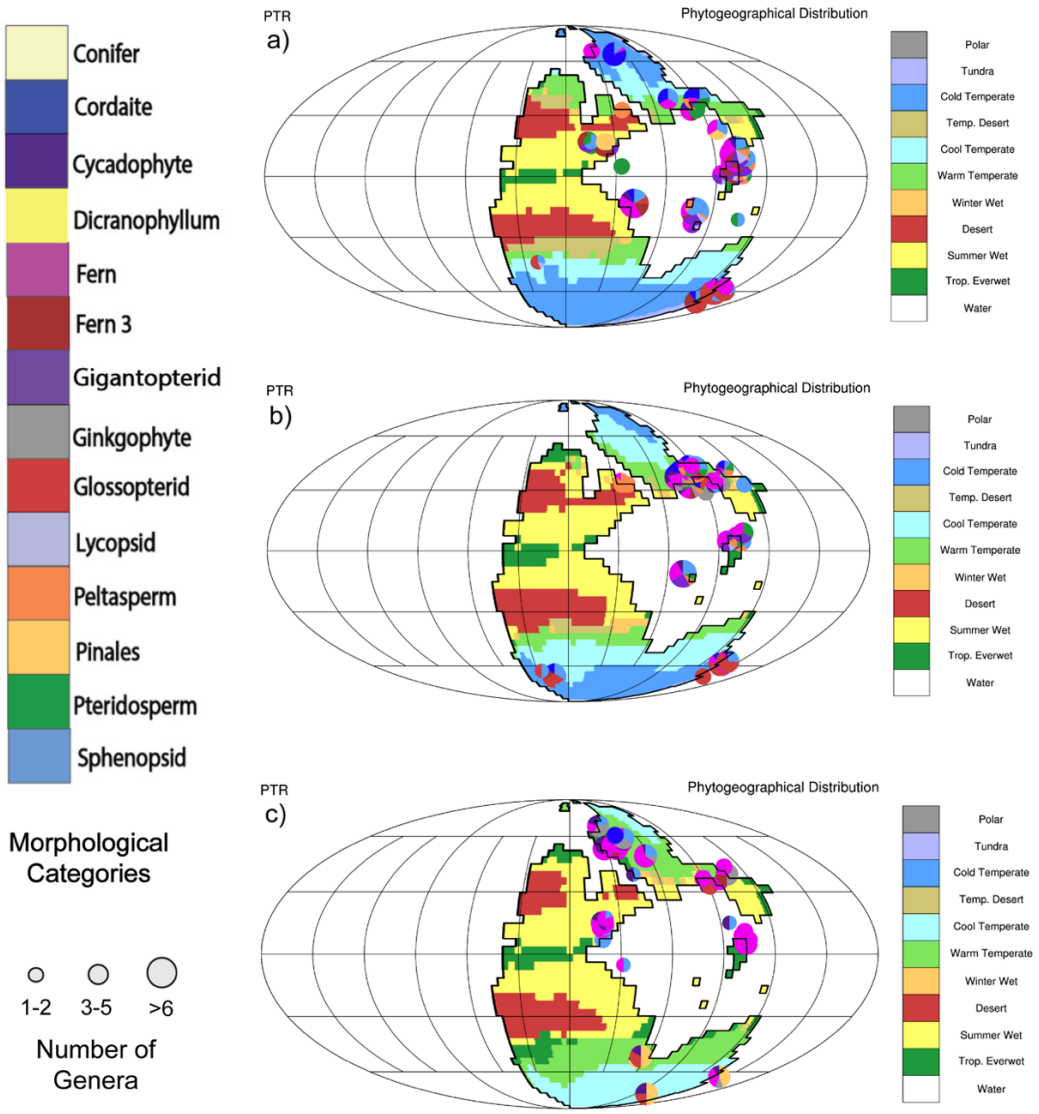

Figure 4.2.1. Phytogeographic distribution during Wuchiapingian (a), Changhsingian (b), and Early Triassic (c) derived using plant-fossil data. The pie-charts are overlain on the biomes simulated from CCSM3 model developed by NCAR for 4x CO_2 (a), 12.7x CO_2 (b), and 12.7x CO_2_WC (c) respectively. The size of the pie-charts represents the diversity of the flora.

4.3 Correspondence Analysis

The following section describes the results from the statistical analyses of the data. The analyses of floral data have been done at the coarser genus level to increase the probability of the data being accurately identified. The summary table (Table 4.3.1. and 4.3.2.) from the analyses of the Wuchiapingian and early Triassic stage suggests the data to be statistically correlated. The significance (p-value) is 0.000 which suggests that the probability of the genera and localities co-occuring with each other by chance is 0%. Also, the first three axes account for most the variance (cumulative of 80.8% for the Wuchiapingian and 86.5% for the Triassic stages respectively).

From the corresponding genus and locality plots, the degree of association between the repective variables can be inferred. Figure 4.3.1. shows the correspondence analysis results for axis 1 versus axis 2 for the genera and localities of Wuchiapingian stage. The Cathaysian localities south China, north China as well Turkey from the data, are centered near the near coordinate axis. The southern Gondwanan sites (Australia and Brazil) have higher scores on axis 1 and low score on axis 2. The northern Angaran sites have been separated from the southern localities with higher score on axis 2 and a low score on axis 1. The only discrepancy is the European locality plotting away from the other Cathaysian localities with a very low score on axis 1 and 2. Associated with the Cathaysian localities are Ferns like Gigantopteris, Pecopteris and Sphenopteris, Pteridosperm like Callipteridium, Sphenopsids like Calamites, Annularia, Paracalmites, Schizoneura, Sphenophyllum and Peltasperms all plotting low on both axes and preferring a tropical to summer-wet climate in common. Europe being a part of Cathaysian realm yet plotting away form its related localites, shows an association with Pinales and Gigantopterids, respectively that have very low scores on axis 1 and 2. However, since the Cathaysian flora comprises of Sphenopisds and Ferns like the Gondwana flora, they plot relatively close to each other. The Gondwanan flora like Glossopteris, Gangamopteris, Schizoneura plot high on axis 1 but low on axis 2 associated with Autralia and Brazil. The genera like

Glottophyllum, Leophyllum, Rufloria belonging to Cordaites, and Fern like Pecopteris plot closer to the Angaran localities, as has been suggested in the section of phytogeographical distribution. These floras plot high on both axes.

The Cathaysian localities of early Triassic stages have very low axis 1 and axis 2 scores (see Figure 4.3.2.). However, north and south China donot plot as closer to each other despite their low scores. This is possibly due to the relatively higher diversity found across north China compared to south China as also suggested in the section of phytogeographical analysis during the early Triassic stages. The floras found in south China mainly comprises of Ferns, whereas north China also comprises of some Sphenopsids like Phyllotheca, Glossopterids like Gangamopteris as well as Cycadophyte like Taeniopteris that plot low an axis 1 but has higher scores on axis 2 as compared to south China.

The Russian locality plot relatively higher (closer to 0) on axis 1 and higher on axis 2 that has Ferns like Cladophlebis, Pecopteris and Sphenopteris, Sphenopsids like Annularia and Sphenobaiera co-occuring with it. The Gondwanan localities are separated from the other localities with higher score on axis 1 and a lower score on axis 2. However, despite a closer association in terms of floristic diversity and location, Autralia plots further from India and Antarctica. These discrepencies can be due to its higher similarities in terms of the genera with Russia than India and Antarctica. It is to be noted that these localities show an association with Cycadophytes and Peltasperms. However, in addition, Australia comprises of Ferns and India/Antarctica comprise of Glossopterids. Hence, Rhabdotaenia (Glossopteris) and Dicroidium (Peltasperm) have hugh axis 1 scores but, low axis 2 scores plotting closer to the latter.

Table 4.3.1. Statistical results for Correspondence analysis of genera from Wuchiapingian localities.

Summary						
Dimension	Singular Value	Inertia	Chi Square	Sig.	Proportion of Inertia	
					Accounted for	Cumulative
1	0.913	0.833			0.361	0.361
2	0.734	0.539			0.234	0.594
3	0.702	0.492			0.213	0.808
4	0.423	0.179			0.077	0.885
5	0.397	0.157			0.068	0.953
6	0.328	0.108			0.047	1.000
Total		2.308	1008.588	0.000[a]	1.000	1.000

Table 4.3.2. Statistical results for Correspondence analysis of genera from early Triassic localities.

Summary						
Dimension	Singular Value	Inertia	Chi Square	Sig.	Proportion of Inertia	
					Accounted for	Cumulative
1	0.836	0.699			0.314	0.314
2	0.795	0.632			0.284	0.598
3	0.770	0.593			0.266	0.865
4	0.390	0.152			0.068	0.933
5	0.298	0.089			0.040	0.973
6	0.246	0.061			0.027	1.000
Total		2.225	440.550	0.000[a]	1.000	1.000

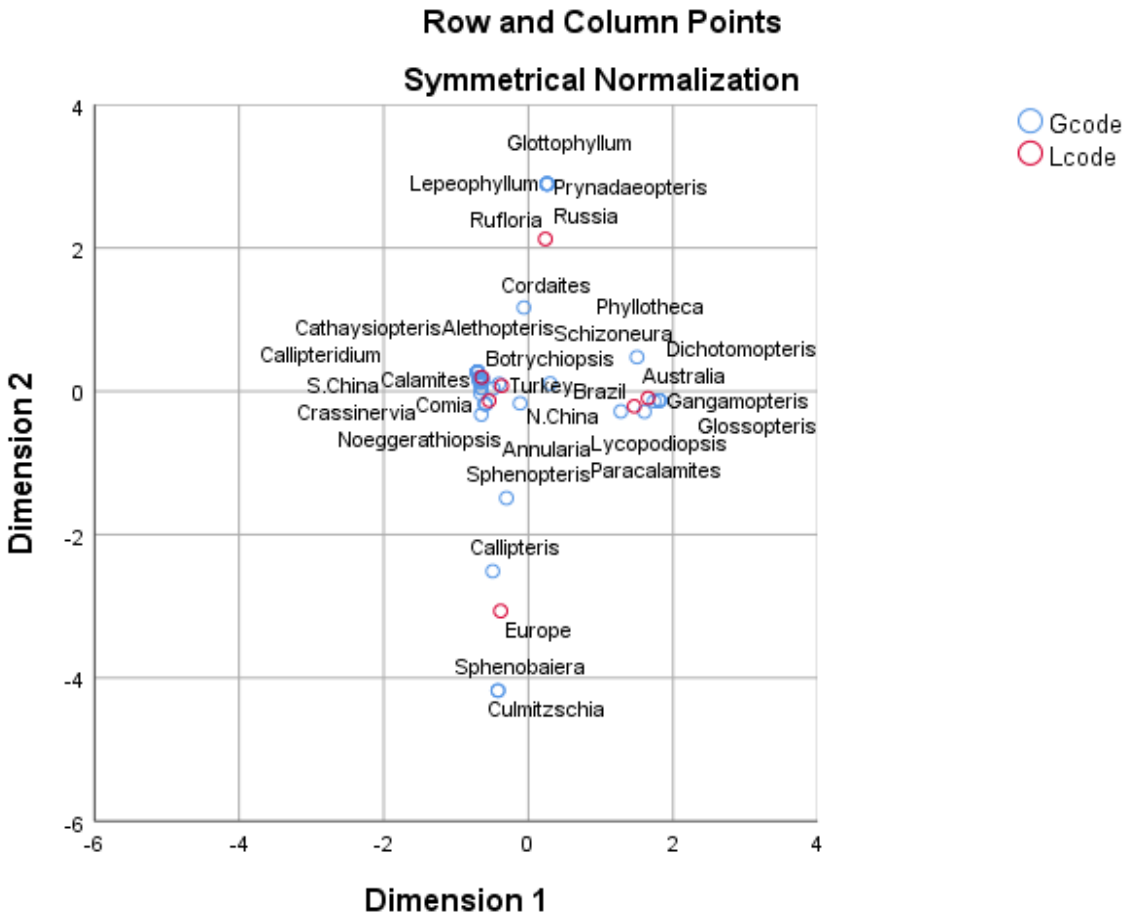

Figure 4.3.1. Wuchiapingian genera and localities showing axes 1 and 2 scores from Correspondence analysis.

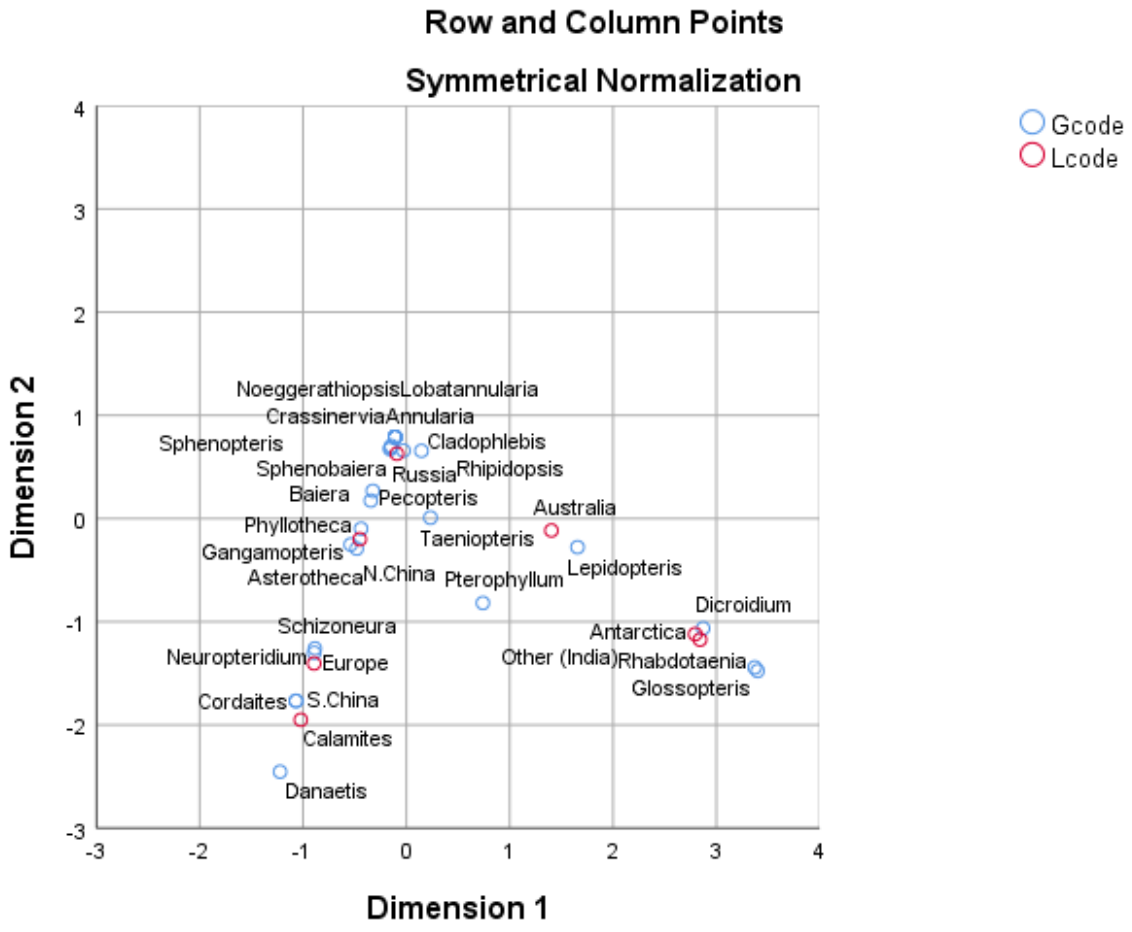

Figure 4.3.2. Early Triassic genera and localities showing axes 1 and 2 scores from Correspondence analysis.

Chapter 5

Discussion and Conclusion

The present study attempts to investigate the end-Permian mass extinction using CCSM3 climate sensitivity experiments (with 4x PAL CO_2, 12.7x PAL CO_2, and 12.7x PAL CO_2 with thinner clouds) which are compared to the plant-fossil data. The corresponding scenarios are based on the carbon estimates from the previous studies, and the proposition of a lower cloud optical depth leading to hothouse climate by Winguth et al. (2015) and are expected to represent the respective Wuchiapingian, Changhsingian and Early Triassic time intervals. The surface temperatures show a substantial increase in the extreme surface air temperature over the Pangea for 12X PAL CO_2_ WC simulation. These contrasts are likely to be attributed to the increased continentality during the Permian. We see a higher seasonality in the southern hemisphere compared to the northern hemisphere, owing to the larger continental mass. To conclude, the surface temperatures show a substantial increase with higher levels of greenhouse gases leading to a weakening of winter temperature and the summers getting warmer. The increased continentality also produces higher evaporation rates with the long overland trajectories causing a depletion of atmospheric moisture.

With the increased radiative forcing, the hydrological cycle is amplified with an enhanced monsoonal precipitation over the equator and higher latitudes. As a result, large arid continental interiors and seasonally stressed regions around the tropical equatorial zone are formed.

The biomes simulated for the radiative forcing, based on the simulated temperature and precipitation, show a shrinking/disappearance of cold temperate biomes at the higher latitudes. This is suggestive of the warming of the higher latitudes with increase in the greenhouse gas concentrations, as we moved into the hothouse world. Consequently, we see the cold temperate biomes being replaced by the cool and warm temperate biomes with

increased CO_2 levels. The seasonality of temperature and precipitation observed also explains the expansion of desert as well as summer-wet biomes simulated over Pangea.

Although the simulated biomes agree reasonably well with the biogeographic distribution of the floral data, future simulations using a higher-resolution model may provide magnified projections for the precipitation and temperature trends across PTB. Hence, an accurate understanding of the processes and climate feeedbacks can be achieved with better resolution of coastal as well as small-scale mountain regions. In addition, the model simulations due to a constant togographic conditions for all stages may have its own limitations. However, feedbacks related to the changes in vegetation can be studied by incorporating a dynamic vegetation model. Thus, the accuracy of the simulated climates can be improved.

The terrestrial vegetation is considered as a potential paleo-climate proxy owing to its sensitivity to the environmental changes. The reconstruction of climate across the PTB by deriving the phytogeographic patterns suggests a decline in diversity. Although, the flora does not show a distinct shift in patterns, a spread of versatile and adaptive flora like Cordaites, Sphenopsids, Ferns and Gigantopterids that can withstand seasonal stresses. A dominance of ferns, spehnopteris, peltasperms, along the regions with accelerated rainfall, especially the tropics and some of the higher latitudes can be inferred. From the observations, the simulated biomes (and the climate conditions) cohere well with the reconstructed floristic patterns. However, it seems that the vegetation that persited through the transition into the hothouse world was not specific to one climatic condition. For example, Ferns, usually belonging to regions of tropical climate, were extended to warm temperate regions too. Similarly, Sphenopsids, usually confined to lower latitudes were extended to higher latitudes forming the ground cover (Rees et al., (2002). It seems that these floras showed adaptations due to different forms (eg: herbaceous) that could exist in, in a wide range of climatic conditions.

It is to be noted that the decline in diversity observed while moving towards the early

Triassic time interval, can probably explain the extinction trend. However, it also possible that the evidences of other data were eliminated as a result of poor preservation due to the cataclysmic events. Only the regions with annual temperatures >10°C with sufficient humidity foster the fossilization of plant matter. In contrast, fossilization rates are much slower in deserts or cool temperate zones. The floral data thus has its own limitations due to the diagenesis and preservation bias. In sections like north China and Angara, a recurrence of flora is observed. Hence, it is possible, owing to the relative stability of the genera, as observed from the datasets as well as a slow emergence of new plants groups post the early Triassic interval, as also suggested by various studies, the so-called 'extinction' was merely and evolutionary succession of the tolerant-species. However, whether or not it is true, is still open for debate and offers more opportunities for research into the topic.

It is integral for the consideration of the derived floristic patterns to ensure the authenticity of the correlation between the climatic conditions affecting the distribution of biomes. From the analysis, the data is found to have be statistically significant as the probability of null hypothesis being true is 0% nullifies the null hypothesis. Hence, the alternative hypothesis hold to be true which suggests an association between the two variables. The statistical analysis not only justifies the use of floral data for deriving the floristic patterns but also, provides a means for an easy interpretation of the associations between the genera and localities. It also allows a better interpretation of discrepencies in the floristic patterns. Most genera found in respective localities cohere well with the expected climate conditions and the simulated biomes. The exceptions include the occurrence of Glossopteris in Antarctica and India- the Gondwanan localities during early Triassic, possibly due to an inaccuracy in the interpretation of the fossil, despite the claims of its extinction from previous studies. Also, although Europe plots away from other Cathaysian localities, it is not unrelated. The discrepencies can be due to the different genera present belonging to the same morphological categories as the ones found in north

America, Turkey and may be China too. As specified earlier, we see a closer association between the localities sharing more genera in common. Similarly, the genera that plot closer together belong to same or close-related morphological categories. However, the errors due to indentification of the specimen, mis-classification and errors in dating that could be entailed while using the fossil data cannot be ignored.

In conclusion, due to the similarities in the observed between the low-resolution model simulations and the floristic patterns, the sensitivity experiments used to predict the conditions across the PTB shows a reasonable agreement. Nevertheless, supplementing the current biome reconstructions with the climate-sensitive data will provide more accurate climate reconstructions across PTB which can be compared with high resolution model simulations.

Chapter 6

References

Basu, A.R., Petaev, M.I., Poreda, R.J., Jacobsen, S.B., and Becker, L., 2003. Chondritic meteorite fragments associated with the Permian-Triassic boundary in Antarctica. Science, v. 302, p. 1388-1392.

Becker, L., Poreda, R.J., Basu, A.R., Pope, K.O., Harrison, T.M., Nicholson, C., and Iasky, R., 2004. Bedout: a possible end-Permian impact crater offshore of Northwestern Australia. Science, v. 304, no. 5676, p. 1469-1477.

Barth, M. C., P. J. Rasch, J. T. Kiehl, C. M. Benkovitz, and S. E. Schwartz, 2000: Sulfur chemistry in the National Center for Atmospheric Research Community Climate Model: Description, evaluation, features and sensitivity to aqueous chemistry. Journal of Geophysical Research, v. 105, p. 1387–1415.

Bonan, G. B., and S. Levis, 2006. Evaluating aspects of the Com- munity Land and Atmosphere Models (CLM3 and CAM) using a dynamic global vegetation model. Journal of Climate, v. 19, p. 2290–2301.

Campbell, I.H., Czamanske, G.K., Fedorenko, V.A., Hill, R.I., and Stepanov, V., 1992. Synchronism of the Siberian traps and the Permian-Triassic boundary: Science, v. 258, no. 5089, p. 1760-1763.

Collins, W.D., Bitz, C.M., Blackmon, M.L., et al., 2006. The Community Climate System Model Version 3 (CCSM3). Journal of Climate, v. 19, p. 2122-2143.

Collins, W.D., Rasch, P.J., Boville, Hack, J.J., McCaa, J.R., Williamson, D.L., Briegleb B.P., Bitz, C.M., Lin, S,J., Zhang, M., 2006. The formulation and atmospheric simulation of Community Atmosphere Model Version 3 (CAM3). Journal of Climate, v. 19, p. 2144-2161.

Erwin, D.H., 1994. The Permo-Triassic extinction. Nature, v. 367, p. 231-236.

Erwin, D.H., 2006. Extinction: How life on Earth nearly ended 250 million years ago. Princeton, New Jersey, Princeton University Press, p. 296.

Glasspool, I.J., Hilton, J., Collinson, M.E., Wang, S., and Li-Cheng-Sen, 2004. Foliar physiognomy in Cathaysian gigantopterids and the potential to track Paleozoic climates using an extinct plant group. Paleogeography, Paleoclimatology, Paleoecology, v. 205, no. 1–2, p. 69-110.

Gent, P. R., F. O. Bryan, G. Danabasoglu, K. Lindsay, D. Tsumune, M. W. Hecht, and S. C. Doney, 2006. Ocean chlo- rofluorocarbon and heat uptake during the twentieth century in the CCSM3. Journal of Climate, v.19, p. 2366–2381.

Gulbranson, E.L., Isbell, J.L., Taylor, E.L., Ryberg, P.E., Taylor, T.N., and Flaig, P.P., 2012. Permian polar forests: deciduousness and environmental variation. Geobiology, v. 10, no. 6, p. 479-495.

Gulbranson, E.L., Ryberg, P.E., Decombeix, A., Taylor, E.L., Taylor, T.N., and Isbell, J.L., 2014. Leaf habit of Late Permian Glossopteris trees from high-palaeolatitude forests. Journal of the Geological Society, v.171, no. 4, p. 493-507.

Hun, J., Emile-Geay, J., Partin, J., 2017. Correlation-based interpretations of paleoclimate data- where statistics meet past climates. Earth and Planetary Science Letters, v. 459, p. 362-371.

Kaiho, K., Kajiwara, Y., Nakano, T., et al., 2001. End-Permian catastrophe by a bolide impact: evidence of a gigantic release of sulfur from the mantle. Geology, v. 29, no. 9, p. 815-818.

Kajiwara, Y., 1994. Development of a largely anoxic stratified ocean and its temporary massive mixing at the Permian/Triassic boundary supported by the sulfur isotopic record. Paleogeography, Paleoclimatology, Paleoecology, v. 111, no. 3-4, p. 367-379.

Kato, Y., Nakao, K., and Isozaki, Y., 2002. Geochemistry of Late Permian to Early Triassic pelagiccherts from southwest Japan: implications for an oceanic redox change. Chemical Geology, v. 182, p. 15-34.

Kidder, D.L., and Worsley, T.R., 2004. Causes and consequences of extreme Permo-Triassic warming to globally equable climate and relation to the Permo-Triassic

extinction and recovery. Paleogeography Paleoclimatology Paleoecology, v. 203, p. 207-237.

Kiehl, J.T., and Shields, C.A., 2005. Climate simulation of the latest Permian: Implications for mass extinction. Geology, v. 33, no. 9, p. 757-760.

Kump, L.R., Pavlov, A., and Arthur, M.A., 2005. Massive release of hydrogen sulfide to the surface ocean and atmosphere during intervals of oceanic anoxia. Geology, v. 33, no. 5, p. 397-400.

Kutzbach, J.E., and Gallimore, R.G., 1989. Pangaean climates: megamonsoons of the megacontinent. Journal of Geophysical Research, v. 94, p. 3341-3358.

Knoll, A.H., Bambach, R.K., Payne, J.L., Pruss, S., and Fischer, W.W., 2007. Paleophysiology and end-Permian mass extinction. Earth and Planetary Science Letters, v. 256, no. 3–4, p. 295-313.

Manabe, S., and Stouffer, R.J., Spleman, M.J., 1994. Response of coupled ocean-atmosphere model to increasing carbon dioxide. Ambio, v. 23, p. 44-49.

Meyen, S.V., 1987. Fundamentals of paleobotany. London, Chapman and Hall, p. 432.

Oleson, K. W., G. B. Bonan, C. Schaaf, F. Gao, Y. Jin, and A. Strahler, 2003. Assessment of global climate model land surface albedo using MODIS data. Geophysical Research Letters, v. 30, p. 1443.

Osen, A., 2014. Sensitivity of the Permian climate to tectonic and radiative forcing changes: Implications for the mass extinction. Ph.D. thesis, University of Texas at Arlington, Texas, 157 p.

Parrish, J.T., 1993. Climate of the supercontinent Pangea. Journal of Geology, v. 101, p. 215-233.

Payne, J.L., and Clapham, M.E., 2012. End-Permian mass extinction in the oceans. An ancient analog for the twenty-first century? Annual Review of Earth and Planetary Sciences, v. 40, no. 1, p. 89-111.

Rasch, P. J., M. C. Barth, J. T. Kiehl, S. E. Schwartz, and C. M. Benkovitz, 2000. A description of the global sulfur cycle and its controlling processes in the National

Center for Atmospheric Research Community Climate Model, Version 3. Journal of Geophysical Research, v. 105**,** p.1367–1385.

Rees, P.M., Gibbs, M.T., Ziegler, A.M., Kutzbach, J.E., and Behling, P.J., 1999. Permian climates: Evaluating model predictions using global paleobotanical data. Geology, v. 27, no. 10, p. 891-894.

Rees, P.M., Ziegler, A.M., Gibbs, M.T., Kutzbach, J.E., Behling, P.J., and Rowley, D.B., 2002. Permian Phytogeographic Patterns and Climate Data/Model Comparisons. Journal of Geology, v.110, no. 1, p. 827-830.

Rees, P.M., Ziegler, A.M., Kutzbach, J.E., Behling, P.J., and Rowley, D.B., 2002. Permian Phytogeographic patterns and climate data/model comparisons. Journal of Geology v.110, p. 1- 31.

Reichow, M.K., Pringle, M.S., Al'Mukhamedov, A.I., Allen, M.B., Andreichev, V.L., Buslov, M.M., Davies, C.E., Fedoseev, G.S., Fitton., J.G., Inger, S., Medvedev, A.Ya., Mitchell, C., Puchkov, V.N., Safonova, I.Yu., Scott, R.A., Saunders, A.D., 2009. The time and extent of the eruption of the Siberian Traps large igneous province: Implications for the end Permian environmental crisis. Earth and Planetary Science Letters, v. 277, p. 9-20.

Renne, P.R., and Basu, A.R., 1991. Rapid eruption of the Siberian traps flood basalts at the PermoTriassic boundary. Science, v. 253, no. 5016, p. 176-179.

Retallack, G.J., 1995. Permian-Triassic life crisis on land: Science, v. 267, p. 77-80.

Royer, D.L., 2006. CO2-forced climate thresholds during the Phanerozoic. Geochimica et Cosmochimica Acta, v. 70, p. 5665-5675.

Shen, S.Z., et al., 2011. Calibrating the end-Permian mass extinction. Science, v. 334, p. 1367-1372.

Shields, C.A., Bailey, D.A., Danabasoglu, G., Jochum, M., Kiehl, J.T., Levis, S., Park, S., 2012. Low-Resolution CCSM4. Journal of Climate, v. 25, p. 3993-4014.

Smith, R., S. Kortas, and B. Meltz, 1995: Curvilinear coordinates for global ocean models. Tech. Rep. LA-UR-95-1146, Los Alamos National Laboratory.

Stewart, W.N., 1983. Paleobotany and evolution of plants. Cambridge, Cambridge University Press, p. 405.

Svensen, H., Planke, S., Plozov, A.G., Schmidbauer, N., Corfu, F., Podladchikov, Y.Y., and Jamtveit, B., 2009. Siberia gas venting and the end-Permian environmental crisis. Earth and Planetary Science Letters, v. 277, p. 490-500.

Walter, H., 1985. Vegetation of the Earth and ecological systems of the geo-biosphere: Berlin, Springer-Verlag, p. 318.

Whittaker, R.H. 1975. Communities and Ecosystems. 2nd Revise Edition, MacMillan Publishing Co., New York, p. 385.

Wignall, P.B., 2001. Large igneous provinces and mass extinctions. Earth-Science Review, v. 53, p. 1-33.

Wignall, P.B., and Hallam, A., 1992. Anoxia as a cause of the Permian/Triassic extinction: Facies evidence from northern Italy and the western United States: Paleogeography, Paleoclimatology, Paleoecology, v. 93, p. 21-460.

Wignall, P.B., and Twitchett, R.J., 1996. Ocean anoxia and the end Permian mass extinction. Science, New Series, v. 272, no. 5265, p. 1155-1158.

Winguth, A., and Winguth, C., 2013. Precession-driven monsoon variability at the Permian-Triassic Boundary-Implications for anoxia and the mass extinction. Global and Planetary Change, v. 105, p. 160-170.

Winguth, A.M.E., Shields, C.A., and Winguth, C., 2015. Transition into a Hothouse World at the Permian-Triassic boundary - A model study: Paleogeography, Paleoclimatology, Paleoecology, v. 440, p. 316-327.

Yeager, S.G., Shields, C.A., Large, W.G., and Hack, J.J., 2006. The low-resolution CCSM3. Journal of Climate, v. 19, p. 2545-2566.

Ziegler, A.M., 1990. Phytogeographic patterns and continental configurations during the Permian Period. in McKerrow, W.S. and Scotese, C.R., eds., Palaeozoic Paleogeography and Biogeography: Bath, UK, Geological Society of London, no.12, p. 363-379.

Biographical Information

Mitali Dinesh Gautam from the EES department of University of Texas at Arlington has pursued her master's studies in Environmental Sciences. Her research into paleo-climate studies was guided by Dr. Arne Winguth and funded by the NSF grant EAR 1636629 as well as College of Science. During her tenure, she received the Fresnel Technologies Graduate Poster Award during the ACES conference held in 2018 at UT Arlington and is currently an active member of Geological Society of America (GSA). She was actively involved to promote sustainability and green initiatives at school and city level while also serving as the president of MavsGoGreen organization on-campus. She has been the first, State of Texas Alliance for Recycling (STAR) Future Leader scholarship recipient. After receiving her master's degree in December 2018, she intends to continue with her Ph.D and contribute to the field of climate research with her studies.